

## Small-angle coherent $\gamma$ -ray scattering for moderate- to high-atomic-number elements

D. A. Bradley, C. S. Chong, A. A. Tajuddin, A. Shukri, and A. M. Ghose

*School of Physics, Universiti Sains Malaysia, 11800 USM Penang, Malaysia*

(Received 27 September 1989; revised manuscript received 27 December 1989)

An annular-ring scattering geometry has been adopted to allow for scattering in the angular range  $5^\circ$ – $15^\circ$ . Measurements are made of differential coherent scattering cross sections of 279- and 662-keV  $\gamma$ -ray photons for Cu, Sn, and Pb. A critical dependence of photon attenuation upon transverse target thickness, demanding target thicknesses considerably less than one mean free path, is confirmed. Comparison of the results of experiment, with state-of-the-art theoretical predictions based upon a second-order perturbative approach, show comprehensive agreement to within the stated experimental-error limits.

### INTRODUCTION

Rayleigh scattering, more definitively known as elastic photon scattering by bound atomic electrons (EPSBE), forms the dominant contribution to the elastic scattering amplitude for x rays, low-energy  $\gamma$  rays, and higher-energy  $\gamma$  rays at nonbackward angles. The development and application of the second-order  $S$ -matrix code of Kissel *et al.*<sup>1</sup> has led to precision,  $O(1\%)$ , total-atom, differential-in-angle EPSBE predictions which generally find good agreement with the results of experiment. Concern arises, however, in making comparisons for  $\gamma$ -ray experiments within the low-momentum-transfer region,  $x \lesssim 10 \text{ \AA}^{-1}$  [where  $x = \sin(\psi/2)/\lambda$ ,  $\lambda$  being the photon wavelength in  $\text{ \AA}$  units and  $\psi$  the scattering angle], where sizable ( $>20\%$ ), nonsystematic departures from agreement between theory and experiment have been noted by Bradley and Ghose.<sup>2</sup> The situation has been discussed in detail by Sen Gupta *et al.*<sup>3</sup>

We mention, in the above connection, an earlier study performed by Bradley and Ghose<sup>4</sup> on Sn and Pb targets for photon energies 279.2 and 661.6 keV and angles of scattering of  $10^\circ$  to  $60^\circ$ . At  $10.5^\circ$ , the only data point investigated for angles of scattering less than  $20^\circ$ , a sizable discrepancy ( $>20\%$ ) was noted between experiment and the available state-of-the-art prediction. Lack of indication of any systematic departure from agreement elsewhere (Sen Gupta *et al.*)<sup>3</sup> has prompted us to reevaluate the situation through the making of new measurements in the angular region of scattering  $10.5^\circ$ . The opportunity to extend the investigated range of scattering angles and targets has also been taken so that in addition to data for Sn and Pb at 661.6 keV (Bradley *et al.*)<sup>5</sup> data for Cu at 661.6 keV and Cu, Sn, and Pb at 279.2 keV at angles of scattering of  $5^\circ$  to  $15^\circ$  are also now made available. It is to be noted that relatively few high-resolution detector measurements exist within this regime and no measurements at energies of less than 1332 keV (other than those of this group) would appear to be presently available as a result of the utilization of a target-reflection-type geometry (to be discussed in the following section). Thus we attempt to evaluate this particular geometry, in the form of an annular target arrangement, with the view of

attaining accurate,  $O(10\%)$ , measured differential cross sections.

Results will indicate that the earlier referred-to discrepancy at  $10.5^\circ$  is almost certainly due in large part to incomplete account being made of rapidly increasing target attenuation with a decrease in scattering angle for scattering angles below  $20^\circ$ .

### SCATTERING GEOMETRY

Broad division can be made into the target-transmission and target-reflection-type geometries (Kane *et al.*)<sup>6</sup> The distinction is to some extent arbitrary since both geometries call for account of target attenuation.

A target-transmission geometry would typically involve reception and transmission, by a thin target, of a highly collimated pencil beam of photons. For small-angle scattering (which for the purposes of this paper we shall understand to mean angles of the order of  $15^\circ$  or less) a large target-to-detector separation is generally necessary in order to provide limitation on reception of nonscattered transmitted photons and to provide sensitivity to change in scattering angle. The overall situation of small scattering volumes and radical collimation militates against the use of small-activity sources with some experimenters utilizing source activities of the order of a few Ci. However, attenuating path lengths at small and moderate angles of scattering are easily accounted for within the target.

A target-reflection-type geometry would typically involve the location of a scattering surface on the Thales circle described between source and detector. Axial symmetry provides the potential for a complete surface-of-revolution target<sup>4</sup> or, less radically, for an annular-target arrangement. The consequent advantages in terms of achievable coherent-scattering signal strength for well-controlled target thickness are demonstrable for moderate to large angles of scattering. Source activities, typically of the order of 100 mCi or less are generally utilized. For small angles of scattering sensitivity to change in scattering angle generally calls for a large source-to-detector separation while limitation of reception of photons not suffering coherent scattering in the target calls,

in the most basic form, for the use of a relatively massive primary-beam shadow bar. A variant of the technique, the multisection filter, has been discussed elsewhere.<sup>7</sup> Use of the shadow bar generates parasitic scattering demanding careful consideration in design and dimensions of the bar in an effort to limit signal degradation (Bradley *et al.*<sup>5</sup>). An additional controlling factor concerns careful account of target-related attenuating path lengths at small angles of scattering; it is apparent from findings to be reported herein that transverse target thicknesses reducing below the confines of the often adopted 40% of one mean-free path (mfp) are required (see, for instance, Kane *et al.*<sup>6</sup>).

The present study builds on earlier investigations by this group involving the use of a surface of revolution geometry (Bradley and Ghose<sup>4</sup> and Bradley *et al.*<sup>8</sup>). Such a geometry, useful for moderate to high-energy photons (of the order of an MeV) at moderate to large angles of scattering (of the order of 20° and above) where signal strengths rapidly reduce, is not the most obvious choice of geometry at smaller angles of scattering. Rapidly increasing differential cross sections with decrease in scattering angle and the difficulty of accurate angular definition imply a requirement for a less extensive surface of scattering and for radically improved positional control of target. We have chosen to use an annular-target arrangement (Fig. 1) with a view to attaining an acceptably good signal-to-background ratio while using a moderately low activity source. A further choice has been the adoption of a parallel-sided shadow bar in an attempt to limit the extent of detectable parasitic scattering; the popular double-cone arrangement is in fact found to act as an efficient producer of small-angle incoherent scattering resulting in significant masking of otherwise resolvable coherent and incoherent peaks (Bradley *et al.*<sup>5</sup>). The sensitivity of signal strength to positional

uncertainties has been made small by choosing a source-to-detector separation of 2 m (providing of the order of 1° cm<sup>-1</sup> sensitivity to change in target radius).

Alignment of the various components, viz., the source, scatterer, and detector assembly, along the zero-angle direction has been achieved to within  $\pm 0.1$  mm using a cathetometer (an optical-beam-aligning aid); collimation apertures and scattering-geometry-component dimensions have allowed definition of scattering angle to within  $\pm 0.1^\circ$ . Positional uncertainties in fact produce an uncertainty in scattering angle of comparable magnitude to that attained in verifying scattering angles from Compton peak positions.

For each scattering angle targets were centrally displaced between source and detector. Source collimation was designed to limit scattering angles to the order of 15°, in order to minimize nontarget scattering in surrounding structures. Fast-screen x-ray films have been used at both 279 and 662 keV to enable characterization of beam extent and also to examine for the possibility of incident-beam inhomogeneity over the plane containing the target.

In accord with usual practice we have used a stepped-down conical detector-collimator arrangement in order to restrict reception of small-angle collimator-scattered photons while imposing minimal restriction on reception of target-scattered photons.

#### SYSTEM PERFORMANCE

The source of 662-keV photons was a nominal 100 mCi of <sup>137</sup>Cs incorporated in a glass bead of 3 mm diameter. The source of 279-keV photons was a nominal initial 50 mCi of <sup>203</sup>Hg in the form of 1.6 g of HgO powder in a sealed quartz ampoule. Detection of scattered photons was accomplished using a 60-cm<sup>3</sup>, horizontally mounted,

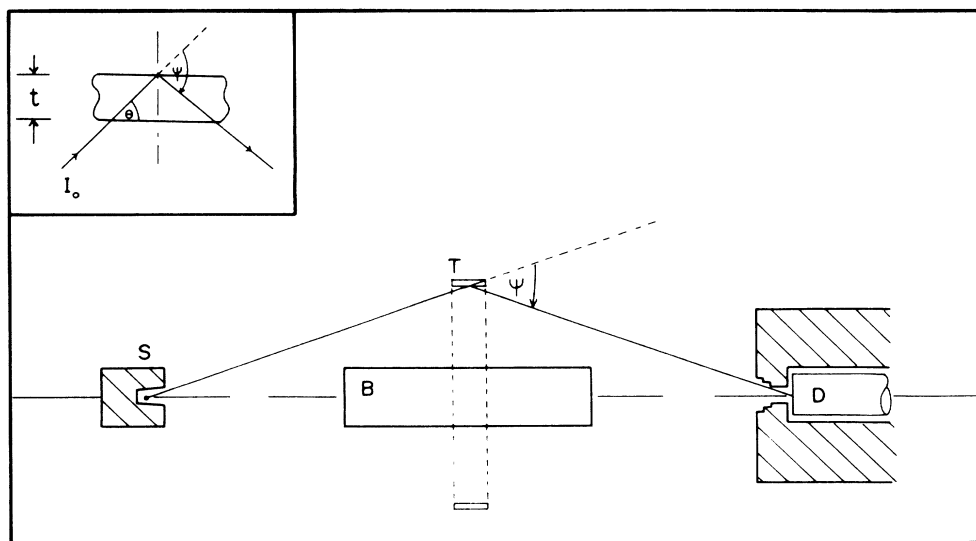


FIG. 1. Annular-ring reflection geometry used in obtaining present measurements (*S*, source; *B*, shadow bar; *T*, target;  $\psi$ , scattering angle, equal to  $2\theta$  in text; *D*, detector). Inset is shown an enlarged view of scatterer and details of the scattering geometry referred to in the text.

coaxial Ge(Li) detector and a 1024-channel multichannel analyzer. At 662 keV a photon-energy sensitivity calibration of 0.5 keV per channel was adopted producing a Compton peak shift of the order of 5 channels for every degree increase in scattering angle for angles within the range 5° to 15°. At 279 keV a photon-energy sensitivity calibration of 0.25 keV per channel was adopted producing a Compton peak shift of the order of 2 to 3 channels for every degree increase in scattering angle. All scattering angles were verified by appealing to the greater angular sensitivity obtained from the 662-keV photon-energy calibration.

The reduction in detected parasitically scattered photons obtained when using a parallel shadow bar in preference to a double-cone arrangement has been discussed elsewhere (Bradley *et al.*<sup>5</sup>) in connection with studies at 662 keV for Pb and Sn. The relative increase in observable incoherent scatter production obtained when using a 279-keV source has led to the choice of an even larger diameter shadow bar at this photon energy. The consequent reduction of the sensibly available range of forward angles (constrained by the attempt to attain sufficiently good signal-to-background ratios using a relatively low activity source) has meant, for this particular setup, restriction at 279 keV, to scattering angles from 8° up to about 15°, with a separation of target and shadow bar at 8° of the order of 2 cm. The use of a smaller diameter shadow bar at 662 keV has provided a similar minimum separation for a 6° scattering angle.

Measures taken to limit the effect of a known radial asymmetry in detector response include the application of an averaged response, with corrections not exceeding 4% at any scattering angle in the range 5° to 15° (Bradley *et al.*<sup>5</sup>).

Counting statistics of 2% to 3% were maintained throughout the study, with target-related coherent-scattering events, corrected for source decay and background, remaining with the range of 1000 to 3000 counts for counting times ranging from 20 000 to 30 000 sec.

## TARGETS

Three target atoms were investigated: Cu, Sn, and Pb. Each target was prepared initially to take the form of a parallel strip, subsequently formed into an annulus, with a fixed length for a given angle of scattering; transverse thicknesses utilized in the calculation of differential cross sections were constrained to a maximum of no more than 0.4 mfp. Less massive targets were fabricated by further cold rolling and tailoring to the desired length and width. A minimum of three appropriately chosen target weights were used at each angle of scattering for each of the elements. The actual maximum thicknesses of scatterer used for the Cu, Sn, and Pb targets were 0.902, 0.843, and 0.595 mm, respectively. The investigated range of transverse target thicknesses, for each of the elements, expressed as a fraction of the respective mean-free paths for 279- and 662-keV photons are indicated in Table I where only values at the two extremes of scattering angle are quoted; also listed, in parentheses, are the range of approximate effective path lengths obtained by multiplying by  $\text{CSC } \theta$  where  $\theta$  represents the angle formed between the incident beam and the axis of symmetry (i.e., the half-scattering angle). Note that, in the case of Pb at 279 keV, data for effective path lengths in excess of 0.4 mfp have also been obtained in order to examine the extent of accord between observation and expectation (the expected dependency of scattered-photon intensity upon target mass is discussed in the next section). Measured mass attenuation data for Cu at 279 and 662 keV are due to Sanjeevaiah *et al.*<sup>9</sup> while those for Sn and Pb at the same photon energies are those due to Bradley.<sup>10</sup>

## TARGET-ATTENUATION CORRECTIONS

The present experiment has been designed to allow for target absorption by extrapolating the target-associated elastic-scattered photon intensity to zero mass. Integrating the elastic-scattered photon intensity  $I$ , over scattering elements of finite thickness  $t$  and area  $a$  yields a form

TABLE I. Range of target transverse thicknesses as a fraction of photon mean-free-path (mfp). Values in parentheses refer to approximate effective path lengths (see text).

Target atom Photon energy (keV)	Cu	Sn	Pb
Range of target thicknesses at a scattering angle of 8.2°			
279	0.024–0.050 (0.17–0.35)	0.019–0.045 (0.13–0.32)	0.026–0.064 (0.18–0.45)
Range of target thicknesses at a scattering angle of 15.1°			
279	0.046–0.094 (0.18–0.36)	0.035–0.084 (0.13–0.32)	0.114–0.391 (0.44–1.51)
Range of target thicknesses at a scattering angle of 6.4°			
662	0.009–0.023 (0.08–0.21)	0.006–0.011 (0.05–0.10)	0.007–0.016 (0.06–0.14)
Range of target thicknesses at a scattering angle of 15.1°			
662	0.016–0.06 (0.06–0.23)	0.014–0.047 (0.05–0.18)	0.020–0.072 (0.08–0.28)

$$I = aI_0 n \frac{d\sigma}{d\Omega} \frac{\sin\theta}{2\mu} \left[ 1 - \exp\left(\frac{-2\mu t}{\sin\theta}\right) \right] \quad (1)$$

where  $I_0$  represents the primary source flux over the target plane,  $n$  the number of scattering center per unit volume, and  $\mu$  the linear attenuation coefficient.

Equation (1) can be reexpressed, as a function of the mass  $m$  of the target, in the form

$$I_s = \frac{I_0 S \sin\theta}{2\mu t \rho} \left[ 1 - \exp\left(\frac{-2\mu m}{\rho a \sin\theta}\right) \right], \quad (2)$$

where  $S = n d\sigma/d\Omega$  and  $m = \rho a t$ , with  $\rho$  being the physical density of the scattering medium, such that  $I_s$  represents the elastic-scattered intensity per unit mass of target.

It is of interest to note that in the first approximation of small path length  $2t \csc\theta$ , the relation reduces to a linear form

$$I_s = \frac{I_0}{\rho} S \left[ 1 - \frac{\mu m}{\rho a \sin\theta} \right]. \quad (3)$$

For a given element, for all presently measured scattering angles, values of  $I_0$  and  $\mu$  remain practically constant. The approximation to small path lengths remains practically valid for all target atoms when using 662-keV photons. Approximate validity is also found at 279 keV for elements up to and inclusive of Sn, variations of  $I_s$  with  $m$  yielding a family of curves of the form of Fig. 2. Thus it is apparent that, for a given element, comparison of intercepts yields ratios of differential cross sections while ratios of gradients depend upon relative values of  $[(d\sigma/d\Omega)/a \sin\theta]$ .

For low scattering angle, low photon energy, high atomic-number target media the approximation to small path lengths is less easily satisfied. Thus in the case of the scattering of a 279-keV photon by Pb, at the smallest scattering angles investigated, extrapolation to zero mass is more accurately provided for by applying a multiplicative correction term derived from Eq. (2), to the measured intensity of target-produced coherent scattering, with the term taking the form

$$(I_s)_0 = I_s \left[ \frac{2\mu m / (\rho \sin\theta)}{a \{ 1 - \exp[-2\mu m / (\rho a \sin\theta)] \}} \right], \quad (4)$$

where  $(I_s)_0$  represents the extrapolated scattered-photon intensity per unit mass at zero mass. Present measurements, when extended beyond the 0.4 mfp range of target effective path lengths demonstrate accord with such an exponential dependence; several such results are illustrated in Fig. 3.

#### MEASUREMENTS OF DIFFERENTIAL CROSS SECTIONS

Adoption of a particular scattering geometry implies a necessity for account of actual system performance. It should be noted, however, that measurement of absolute differential coherent-scattering cross sections does not formally require measurement of quantities such as source activity, detector solid-angle acceptance and detector efficiencies (both intrinsic and geometrical). An auxiliary source (generally being of substantially lower activity than the primary source) when placed at the primary-source position and also in the plane containing the target can provide a system for cancellation of effects such as nonuniformity of flux over the target plane, in addition to the other quantities mentioned above, by taking appropriate ratios of measurable quantities at the specific angles of scattering investigated. In this way one may avoid what might otherwise constitute potentially significant sources of error. Within this scheme, and for the particular geometry used herein, system characterization has therefore been performed in respect of the following measurable quantities: (i) primary source flux  $I_0$ , over the target plane, using a NaI detector, yielding a measurement  $C_1(I_0)$ ; (ii) auxiliary source flux  $I_a$ , using the same NaI detector in an identical setup to that provided for in (i) above, yielding a measurement  $C_1(I_a)$ ; (iii)

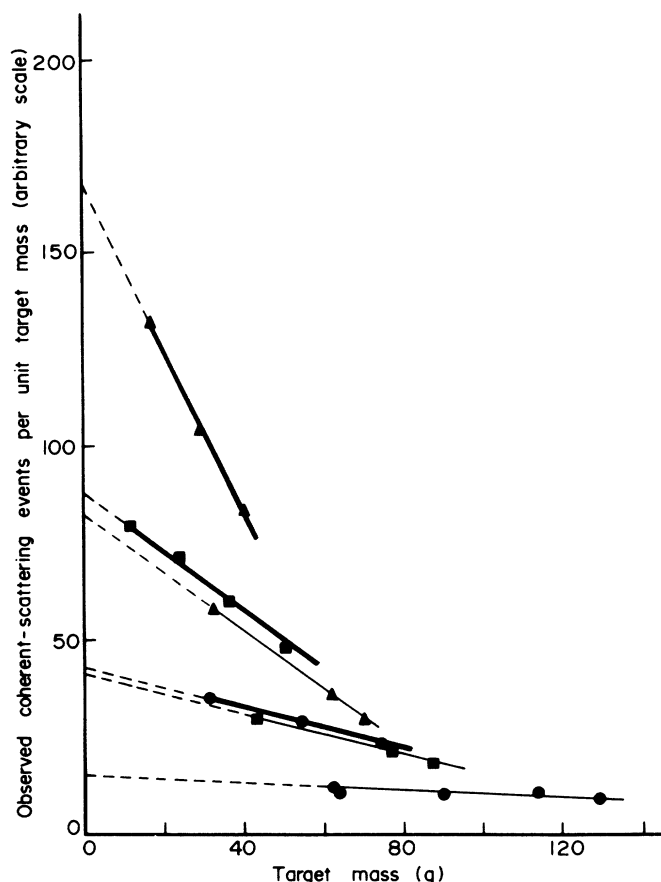


FIG. 2. Variations in coherently scattered photon intensity from Cu and Sn targets as a function of the target mass for various angles of scattering in the range  $8.2^\circ$  to  $15.1^\circ$ . Heavy lines refer to Sn data while lighter lines refer to Cu data;  $\blacktriangle$  refer to data obtained at a scattering angle of  $8.2^\circ$  while  $\blacksquare$  and  $\bullet$  refer to data obtained at scattering angles of  $10.4^\circ$  and  $15.1^\circ$ , respectively. The small-path-length approximation is indicated by use of a dashed line.

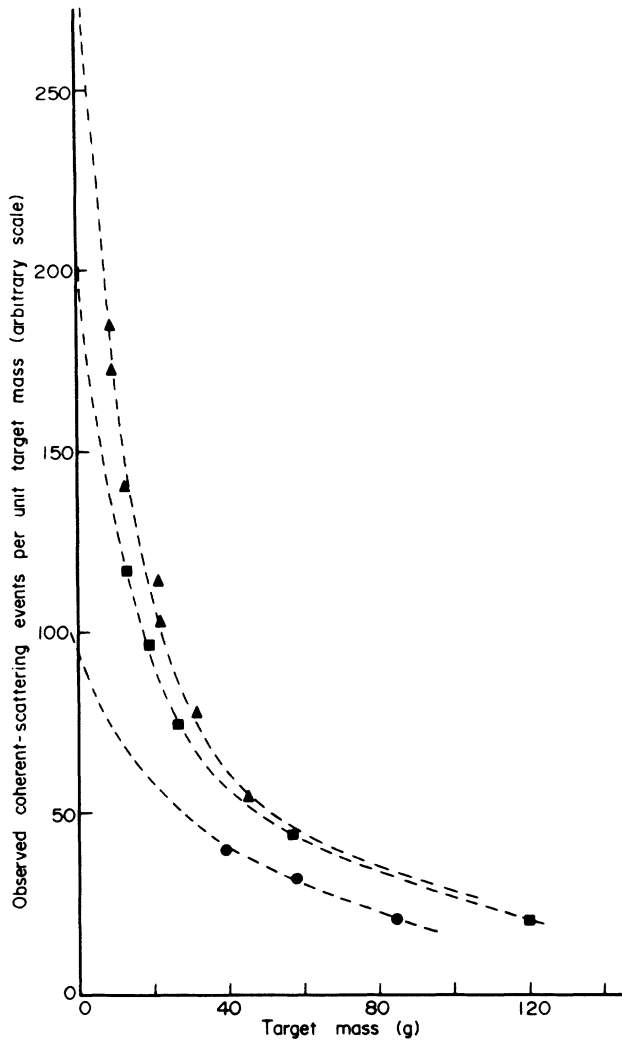


FIG. 3. Variation in coherent photon intensity from Pb targets as a function of the target mass for various angles of scattering in the range  $8.1^\circ$  to  $15.1^\circ$ . (The symbols take on the same representations defined in Fig. 2.) The small-path-length approximation is no longer applicable; extrapolated results obtained by applying the multiplicative correction term (relation 4 in text) are indicated.

the intensity of elastically scattered primary-source photons per unit mass of scatterer, using a Ge(Li) detector, yielding, from application of expression (4), an attenuation-corrected measurement  $C_2(I_s)_0$ ; (iv) auxiliary source flux  $I_a$ , in an arrangement simulating detection of

TABLE II. Experimental differential cross-section values for Cu at 662 keV. Numbers in parentheses refer to  $S$ -matrix-code predictions.

Scattering angle (deg)	$(d\sigma/d\Omega)_{\text{Cu}}$ (b sr $^{-1}$ )
6.4	$0.255 \pm 0.026$ (0.279)
8.2	$0.153 \pm 0.015$ (0.148)
10.4	$0.091 \pm 0.009$ (0.094)
15.1	$0.040 \pm 0.004$ (0.040)

target elastically scattered photons, yielding a measurement  $C_2(I_a)$ . It then becomes apparent that the ratio of elastically scattered photons to the primary-beam intensity on the target, as expressed in relation (2), can be made to include actual system performance characteristics through an appropriate arrangement of indices (i) to (iv). Within these terms calculation of the differential cross section can be reduced to an arrangement of the form:

$$\frac{d\sigma}{d\Omega} = \frac{C_1(I_a) C_2(I_s)_0 A}{C_1(I_0) C_2(I_a) N_A},$$

where  $N_A$  refers to Avogadro's number and  $A$  the atomic weight of the target atom.

## RESULTS AND DISCUSSION

The dominating role of attenuation corrections in heavy targets, for the lower angles of scattering, is illustrated to good effect for the case of 279-keV photons scattering from Pb (Fig. 3). In particular it is evident for photon energies of a few hundred keV or less, scattering off high- $Z$  target media at acute angles of the order of  $10^\circ$  or less, that the annular target geometry is only made effective for the determination of differential scattering cross sections, through careful account of target attenuation. This critical dependency upon sufficient account of target attenuation provides some understanding for one of the possible causes underlying the sometimes significantly lower experimental cross sections reported for lower momentum transfers when making comparison with state-of-the-art theoretical predictions. We note, in particular, that while earlier studies by this group (Bradley and Ghose<sup>4</sup>) indicated a discrepancy with theory for  $10.5^\circ$  scattering off Sn and Pb at 279 keV and 662 keV no such discrepancies were observed at similar momentum transfers and photon energies by other groups using

TABLE III. Experimental differential cross-section values at 279 keV. Numbers in parentheses refer to  $S$ -matrix or interpolated  $S$ -matrix-code predictions.

Scattering angle (deg)	$(d\sigma/d\Omega)_{\text{Cu}}$ (b sr $^{-1}$ )	$(d\sigma/d\Omega)_{\text{Sn}}$ (b sr $^{-1}$ )	$(d\sigma/d\Omega)_{\text{Pb}}$ (b sr $^{-1}$ )
8.2	$1.86 \pm 0.19$ (1.80)	$7.77 \pm 0.78$ (7.55)	$26.1 \pm 2.6$ (25.4)
10.4	$1.01 \pm 0.10$ (0.930)	$4.20 \pm 0.42$ (3.90)	$16.9 \pm 1.7$ (16.5)
12.3	$0.570 \pm 0.054$ (0.542)	$2.79 \pm 0.28$ (2.65)	$11.5 \pm 1.2$ (12.2)
15.1	$0.277 \pm 0.028$ (0.275)	$1.73 \pm 0.17$ (1.75)	$8.20 \pm 0.82$ (7.75)

transmission geometries (where photon path lengths are approximately identical to transverse target thickness).<sup>11,12</sup>

In Tables II and III we provide results of present measurements together with the associated error estimates. In arriving at present error estimates we have taken into account contributory upper-limit uncertainties in measurement of primary-source and auxiliary-source flux over the target plane. Also taken into account are estimates of upper-limit uncertainties in measurement of simulated coherent-scattered photons using the auxiliary source and measurement of actual scattered-photon intensity corrected for target attenuation. Taking these estimates, in quadrature with uncertainties arising from counting statistics, background subtraction, and angular definition, leads us to provide error estimates at the 95% confidence level, that do not exceed 10% or fall anywhere below 5%. As such it is clear that comprehensive agreement is attained to within 10% with state-of-the-art predictions. We note here that while computed *S*-matrix

predictions for Pb, Sn, and several other elements are readily available for a wide range of  $\gamma$ -ray energies (see, for instance Kane *et al.*<sup>4</sup>) predictions for Cu have only more recently been made available for the photon energies of interest herein.

#### ACKNOWLEDGMENTS

The authors are grateful to Paul Bergstrom and Ye Kuang of the University of Pittsburgh for making available theoretical predictions using the *S*-matrix code developed by Lynn Kissel. Computations were performed at the Pittsburgh Supercomputing Center on a CRAY Y-MP/832 under Grant No. PHY-8704088. A great deal of stimulus for this work has derived from the interest of Richard Pratt and Lynn Kissel, to whom we are indebted. Financial support for the experimental study was provided by a grant from the Universiti Sains Malaysia; the interest of Dr. Abdul Latiff Awang is much appreciated.

<sup>1</sup>L. Kissel, R. H. Pratt, and S. C. Roy, *Phys. Rev. A* **22**, 1970 (1980).

<sup>2</sup>D. A. Bradley and A. M. Ghose, *Nucl. Instrum. Methods A* **255**, 59 (1987).

<sup>3</sup>S. K. Sen Gupta, D. A. Bradley, S. C. Roy, and R. H. Pratt, *Trans. Bose Res. Inst.* (to be published).

<sup>4</sup>D. A. Bradley and A. M. Ghose, *Phys. Rev. A* **33**, 191 (1986).

<sup>5</sup>D. A. Bradley, C. S. Chong, A. A. Tajuddin, A. Shukri, and A. M. Ghose, *Nucl. Instrum. Methods A* **280**, 207 (1989).

<sup>6</sup>P. P. Kane, L. Kissel, R. H. Pratt, and S. C. Roy, *Phys. Rep.* **140**, 75 (1986).

<sup>7</sup>A. Nath and A. M. Ghose, *Nucl. Phys.* **57**, 547 (1964).

<sup>8</sup>D. A. Bradley, C. S. Chong, and A. M. Ghose, *Nucl. Instrum. Methods A* **270**, 537 (1988).

<sup>9</sup>B. Sanjeevaiah, S. Gopal, Ramakrishna Gowda, C. Ranganathaiah, and T. K. Umesh, in *Proceedings of the Second International Symposium on Radiation Physics, Penang, 1983*, edited by C. S. Chong, A. M. Ghose, J. H. Hubbell, P. K. Iyengar, D. Jackson, T. Nakamura, R. H. Pratt, J. Rotblat, and D. A. Bradley (Universiti Sains Malaysia, Penang, Malaysia, 1983), p. 146.

<sup>10</sup>D. A. Bradley, Ph.D. thesis, Universiti Sains Malaysia, Penang, Malaysia, 1985.

<sup>11</sup>O. Gonçalves, S. de Barros, M. Gasper, and A. M. Gonçalves, *Z. Phys. D* **1**, 167 (1986).

<sup>12</sup>J. P. Lestone, R. B. Taylor, P. Teansomprasong, and I. B. Whittingham, *Phys. Rev. A* **37**, 3218 (1988).